JACS
JOURNAL OF THE AMERICAN CHEMICAL SOCIETY
pubs.acs.org/JACS
Article

Activation of an Open Shell, Carbyne-Bridged Diiron Complex Toward Binding of Dinitrogen

Charles H. Arnett and Theodor Agapie*

Cite This: J. Am. Chem. Soc. 2020, 142, 10059−10068
Read Online
ACCESS | Metrics & More | Article Recommendations | Supporting Information

ABSTRACT: Binding of N_2 by nitrogenase requires a reductive activation of the FeMo-cofactor, but the precise structure and atomic composition of FeMoco in its activated form is not well understood. However, recent crystallographic studies suggest that N_2 reduction may occur at a carbon-bridged diiron subunit of FeMoco. Toward modeling the activation of a Fe−(μ-C)−Fe site toward N_2 binding, we synthesized a new dinucleating, hexaphosphine ligand derived from a 2,6-disubstituted toluene platform. Activation of the central methyl group of the ligand affords the diiron μ-carbyne complex (P_6ArC)-Fe_2(μ-H) featuring a biologically relevant Fe(μ-carbyne)(μ-H)Fe motif. SQUID magnetometry, Mössbauer spectroscopy, and DFT calculations reveal that (P_6ArC)Fe_2(μ-H) has a well-isolated S = 1 ground state, distinguishing it from all other diiron μ-carbyne complexes which are diamagnetic. Upon the addition of sources of H^+/e^- (H_2, TEMPO-H or HCl), (P_6ArC)Fe_2(μ-H) is activated toward N_2 binding, with concomitant protonation of the carbyne ligand. Although reaction with H_2 ultimately leads to complete protonation of the carbyne moiety, mechanistic investigations indicate that formation of a single C−H bond, with concomitant cleavage of one Fe−C bond, generates an iron-carbene intermediate capable of coordinating N_2.

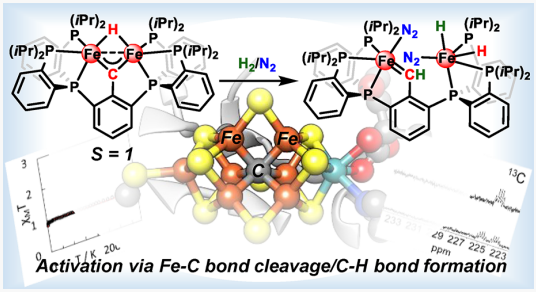

INTRODUCTION

Reduction of atmospheric N_2 by the Mo-nitrogenase enzyme requires an initial activation phase[1]—the active site[7Fe−9S−Mo−C−*R*−homocitrate] cluster[2−5] (the iron molybdenum cofactor, FeMoco, Figure 1, top) must first be reduced by 3−4 electrons before substrate binds. Although pulse EPR measurements indicate that bridging hydrides accumulate on the cofactor during this process,[6,7] the precise structure and atomic composition of FeMoco in its activated form is not well understood.[8,9] Structural rearrangements are common for iron−sulfur clusters,[10,11] and recent crystallographic studies reveal that a μ_2-sulfide ligand in the "belt" region of FeMoco can be displaced to expose a binding site for substrates and intermediates.[12−14] Computational and synthetic modeling studies demonstrate that Fe−S bond cleavage is a feasible mechanism for cofactor activation,[15−17] though even more dramatic rearrangements of FeMoco may be required.[18−20] For example, one computational study suggests that N_2 binds in the central cavity of the cofactor, following protonation of the interstitial carbide to a methyl ligand.[19] Despite ambiguity in the atomic-level details, the foregoing studies intimate a central role for a carbon-bridged diiron subunit of FeMoco in mediating the reduction of N_2.

Synthetic modeling studies have the potential to provide mechanistic insight into the activation of a carbon-bridged

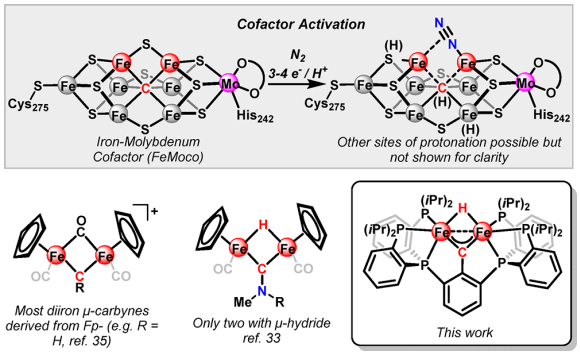

Figure 1. Binding of N_2 by the iron−molybdenum cofactor (FeMoco) of nitrogenase requires reductive activation of the cofactor, resulting in ill-defined structural changes (top). Diiron μ-carbyne complexes are structural models of a carbon-bridged diiron subunit of FeMoco, proposed to be central to catalysis.

Received: February 21, 2020
Published: April 14, 2020

https://dx.doi.org/10.1021/jacs.0c01896
J. Am. Chem. Soc. 2020, 142, 10059−10068

diiron site toward N_2 binding. To date, however, efforts in this regard have been largely restricted to the study of monometallic iron complexes with terminal arene,[17,21] alkyl,[22−24] or carbene-based donors.[25−28] Although these studies have revealed a role for Fe−C hemilability in the activation of N_2,[23,24] they do not address proposals involving carbide protonation and Fe−C bond cleavage or the potential for cooperative N_2 binding to two metals. A number of diiron μ-carbyne complexes have been reported which feature a biologically relevant Fe−(μ-C)−Fe motif,[29−37] although none of these have been studied in the context of biological nitrogen fixation. The vast majority of these complexes are derivatives of the Fp anion and contain multiple π-acidic CO ligands (Figure 1, bottom), rendering the carbyne highly electrophilic.[32,38−44] Moreover, all diiron μ-carbynes reported thus far are closed shell, diamagnetic species, in stark contrast to the paramagnetic nature of FeMoco. In fact, there are only a handful of complexes featuring an Fe−(μ-CR_x)−Fe (x = 2 or 3) motif which exhibit an open shell configuration.[45−49]

Inspired by the mechanism through which the interstitial carbide is installed into FeMoco,[50−52] we envisioned that the Fe-(μ-CR)-Fe linkage might alternatively be accessed by templating two iron centers in the proximity of a methyl substituent, facilitating direct C−H activation. Toward this end, we have designed a dinucleating, hexaphosphine ligand derived from a 2,6-disubstituted toluene platform. Although this phosphine-rich supporting ligand is electronically distinct from the sulfide-rich environment of the iron centers in FeMoco, activation of the central methyl group affords an unusual open shell, carbyne-bridged diiron complex (Figure 1, bottom) which can be activated for binding of N_2 upon addition of H_2.

RESULTS AND DISCUSSION

Template-Assisted Synthesis of a Diiron μ-Carbyne Complex. The desired proligand was synthesized in two steps from 2,6-dibromotoluene (Scheme 1). Lithiation with 1 equiv of *n*BuLi followed by addition of bis(*o*-diisopropylphosphinophenyl)-chlorophosphine (P_2P^{Cl}) yields the triphosphine intermediate P_3ArCH_3 (**1**). Although lithium−halogen exchange of **1** is dominated by self-quenching, generation of the Grignard reagent with Mg followed by treatment with P_2P^{Cl} proceeds cleanly, affording the desired ligand in 81% yield after workup. Metalation of P_6ArCH_3 (**2**) with two equivalents of $FeBr_2$ in tetrahydrofuran precipitates a yellow-green powder, believed to correspond to the diiron(II) tetrabromide complex (P_6ArCH_3)Fe_2Br_4 (**3**, Figure S7 of the Supporting Information, SI). Reduction of **3** with Cp^*_2Co in benzene affords the diiron(I) congener (P_6ArCH_3)Fe_2Br_2 (**4**) as a brick red solid. The iron centers of **4** are four coordinate with Fe−P bond lengths of 2.254(5) Å (Fe1−P1), 2.318(6) Å (Fe1−P2), and 2.330(6) Å (Fe1−P3). Most notably, in the solid state, **4** adopts a geometry appropriate for C−H activation (Figure S9)—both iron centers are directed toward the central methyl group, resulting in a reasonably short Fe1−C1 distance of 3.834 Å (Table S7).

Scheme 1. Ligand Synthesis and Metalation

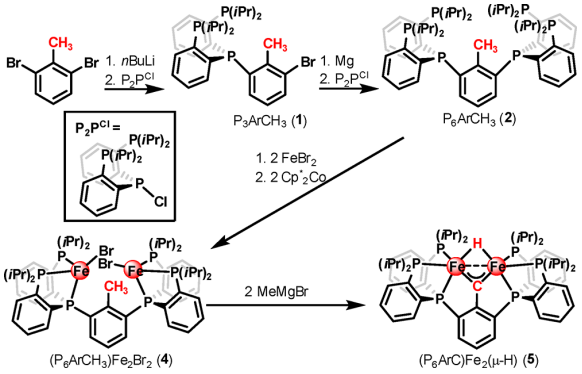

Treatment of **4** with 2 equiv of MeMgBr in tetrahydrofuran followed by refluxing in benzene generates a new paramagnetic species. X-ray diffraction studies revealed the formation of the desired diiron μ-carbyne complex (P_6ArC)Fe_2(μ-H) (**5**, Figure 2). Each iron site of **5** adopts *pseudo*-trigonal bipyramidal geometry with one short Fe−P distance (2.1307(7) Å, Table S7) and two long Fe−P bond lengths (Fe1−P2, 2.2627(8) Å and Fe1−P3, 2.2522(6) Å). Similar to reported carbyne-bridged complexes, **5** features a short Fe1−C1 distance of 1.792(1) Å. Notably, the diffraction data are of sufficient quality to unambiguously locate a single hydride bridging the two iron sites, with an Fe1−H1 bond length of 1.76(3) Å. The Fe−Fe distance within the Fe(μ-CAr)(μ-H)Fe diamond core of **5** is short (2.6776(6) Å), close to the range expected for an Fe−Fe single bond (ave. 2.6(1) Å).[45] To accommodate this short Fe−Fe separation, the ligand framework must distort, resulting in a P1−C3−C4 angle (141.42(1)°) which deviates significantly from the expected value (*c.a.* 120 degrees).

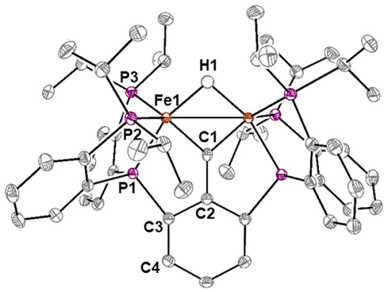

Figure 2. Crystal structure of (P_6ArC)Fe_2(μ-H) (**5**). Hydrogen atoms on the ligand are omitted for clarity. Thermal ellipsoids shown at 50% probability.

Spectroscopic and Computational Characterization of 5. Given the strong-field donor set of **5**, the observation of broad, paramagnetically shifted resonances in its ^{1}H NMR spectrum (Figure S13) is notable. The position of these resonances exhibit ideal Curie behavior between 198−298 K (Figure S15), suggesting an open shell configuration rather than thermal population of a low-lying paramagnetic excited state. Indeed, variable-temperature magnetic susceptibility measurements reveal that the χT value of **5** (1.01 cm^3 K mol^{-1}, 298 K, equivalent to μ_{eff} = 2.84 μ_B) is nearly constant between 5−298 K (Figure 3a), indicating a thermally isolated S = 1 ground state (expected: μ_{eff} = 2.83 μ_B). Although a number of open shell diiron μ-hydride complexes have been reported,[53−59] **5** is the first paramagnetic diiron species featuring a μ-carbyne ligand.

Additional insight into the unusual electronic structure of **5** was obtained from DFT calculations. Consistent with experi-

https://dx.doi.org/10.1021/jacs.0c01896
J. Am. Chem. Soc. 2020, 142, 10059−10068

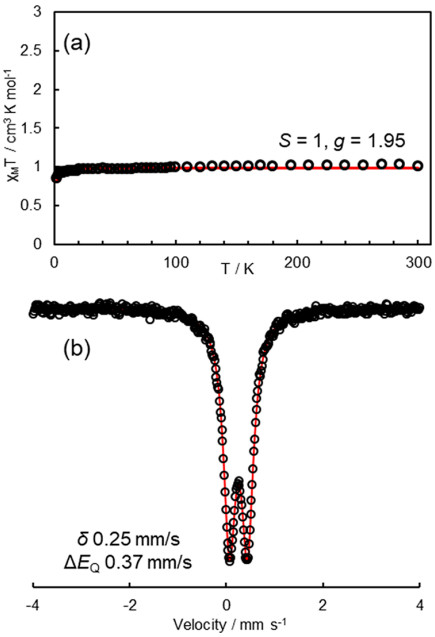

Figure 3. Characterization of $(P_6ArC)Fe_2(\mu\text{-}H)$ (**5**). Variable temperature magnetic susceptibility studies reveal a thermally isolated $S = 1$ ground state (a). ^{57}Fe Mössbauer spectrum (80 K, polycrystalline sample) of **5** (b).

ment, computational studies reveal a triplet ground state for **5** (Table S2) with metrical parameters that closely resemble those in the solid state structure (Table S1). The calculated frontier molecular orbitals include 10 orbitals with significant Fe 3*d* character and nearly equal distribution onto each iron site (Figure S74). As a result of the contraction of the axial Fe1−P1 bond length (Fe1−P1:2.1307(7) Å), the Fe $3d_{xz}$ orbitals are higher in energy than orbitals of Fe $3d_{yz}$ parentage (Figure 4a) which are involved in σ-bonding with the equatorial phosphines (Fe1−P2:2.2627(8) Å and Fe1−P3:2.2522(6) Å). Additionally, the Fe $3d_{xz}$ orbitals are engaged in σ-bonding with both the μ-hydride and μ-carbyne ligands. A single Fe−H−Fe σ bonding orbital can be located below the *d* set (HOMO-9, Figure 4c), leading to a half-bond order for each Fe−H interaction (Löwdin bond order = 0.47). The two Fe−C σ-bonding orbitals are nondegenerate—one is relatively high-lying (HOMO-8), whereas the other is much lower in energy (HOMO-33). Mixing of $3d_{xy}$ character into the symmetric combination of the $3d_{yz}$ orbitals facilitates a highly covalent π bonding interaction with the carbyne ligand (HOMO-7). The presence of strong Fe−C π-bonding results in an empty Fe−C π^* orbital (LUMO, Figure 4b,c) and rationalizes the inaccessibility of higher spin states (e.g., $S = 2$). This orbital analysis implies delocalized multiple bond character, with a formal Fe−C bond order of 1.5 (Löwdin bond order = 1.34).

The antisymmetric combination of the Fe $3d_{yz}$ orbitals (HOMO) does not have appropriate symmetry to interact with either the μ-hydride or the μ-carbyne ligands. As a result of the longer Fe1−P2 and Fe1−P3 distances, this orbital is energetically accessible and is singly occupied (HOMO) in the ground state of **5**. The remaining singly occupied orbital is of $3d_{x2\text{-}y2}$ parentage and has δ-symmetry relative to the Fe−Fe vector (HOMO-1, Figure 4b,c). Five additional iron-based orbitals with predominantly Fe $3d_{xy}$, $3d_{x2\text{-}y2}$, and $3d_{z2}$ character are found with lower energy and are fully populated (Figure S74). These filled orbitals include both the Fe−Fe σ (HOMO-6) and σ^* (HOMO-3) orbitals, suggesting that σ-bonding should not contribute significantly to the Fe−Fe interaction. Rather, the short Fe−Fe separation (2.6776(6) Å) appears to be a consequence of the constrained ligand environment, with electronic communication mediated by 3-center, 2-electron bonding across the Fe−C−Fe and the Fe−H−Fe motifs, leading to an Fe−Fe Löwdin bond order of 0.58.

Validation of this theoretical model can be obtained by comparison of the calculated (δ = 0.24 mm s^{-1}, $|\Delta E_Q|$ = 0.38 mm s^{-1}) and experimental (δ = 0.25 mm s^{-1}, $|\Delta E_Q|$ = 0.37 mm s^{-1}, Figure 3b) Mössbauer parameters, which are accurately reproduced only in the triplet state (Table S3).[60] Assuming a closed shell configuration for the bridging carbyne ligand, the electronic structure of **5** can be formulated as $\{Fe^{II}_2(\mu\text{-}CAr^{3-})(\mu\text{-}H^-)\}$. Under this assumption, the 12 Fe 3*d* electrons occupy molecular orbitals that are delocalized across both iron centers, as well as the ligand. This situation is analogous to that recently described for the formally $Ni^{II}_2(\mu\text{-}H)_2$ dimer $[Cp'Ni(\mu\text{-}H)]_2$ (Cp′ = 1,2,3,4-tetraisopropylcyclopentadienyl), which also adopts an $S = 1$ configuration.[61] However, due to delocalization and covalency, the physical oxidation state of **5** may be lower than Fe^{II}. Although there are few pertinent reference compounds against which the Mössbauer parameters may be benchmarked, the isomer shift of **5** (δ = 0.25 mm s^{-1}) falls between those reported for a related $S = 1$ iron(II)−carbonyl complex $[(SiP_3)Fe(CO)]^+$ (δ = 0.31 mm s^{-1}) and its iron(I) congener $[(SiP_3)Fe(CO)]$ (δ = 0.21 mm s^{-1}).[62] In light of these ambiguities, explicit reference to the formal oxidation state of **5** shall be avoided.

Activation of 5 toward N_2 Binding. Complex **5** is a unique entry point for developing model chemistry relevant to the activation of FeMoco, especially in light of spectroscopic data that indicates bridging hydride ligands accumulate on the cofactor prior to N_2 binding.[6,7] For this reason, we investigated whether addition of H^+/e^- or, alternatively, H_2 promotes coordination of N_2. Exposure of **5** to a roughly equimolar mixture of H_2 and N_2 slowly converges to a single diamagnetic product (Figures S47 and S48) with spectroscopic parameters consistent with $(P_6ArCH_3)Fe_2(H_2)_2(H)_4$(**6-$H_2$**) formulation (Scheme 2). The ^{31}P NMR spectrum of **6-H_2** exhibits two distinct resonances at 124.9 ppm (d, J = 15 Hz, 4P) and 110.0 ppm (t, J = 19 Hz, 2 P). A resonance at −12.9 ppm (t, J = 28 Hz) is observed in the ^{1}H NMR spectrum of **6-H_2** which corresponds to 8 protons (Figure S22). Under an H_2/N_2 atmosphere, these protons relax quickly (T_1 = 48 ms, Figure S25), characteristic of a metal−dihydrogen adduct.[63] Cooling the sample to 198 K partially resolves this signal into three distinct hydridic/Fe−H_2 resonances (Figure S24), suggesting that the hydride/H_2 ligands rapidly interconvert. Although similar reactivity is observed if **5** is exposed to an atmosphere of H_2, the reaction does not proceed cleanly. Significant quantities of dissociated ligand are observed by ^{31}P NMR, implying that N_2 stabilizes one or more of the intermediates.

Complex **6-H_2** is not stable under an atmosphere of N_2, converting gradually to the N_2 congener $(P_6ArCH_3)Fe_2(N_2)_2(H)_4$(**6-$N_2$**, Figures S53−S55). This transformation is accompanied by the loss of the resonance at −12.9 ppm in the ^{1}H NMR spectrum of **6-H_2** and the appearance of new features at −9.8 ppm (2H, T_1 = 382 ms) and −20.5 ppm (2H,

https://dx.doi.org/10.1021/jacs.0c01896
J. Am. Chem. Soc. 2020, 142, 10059−10068

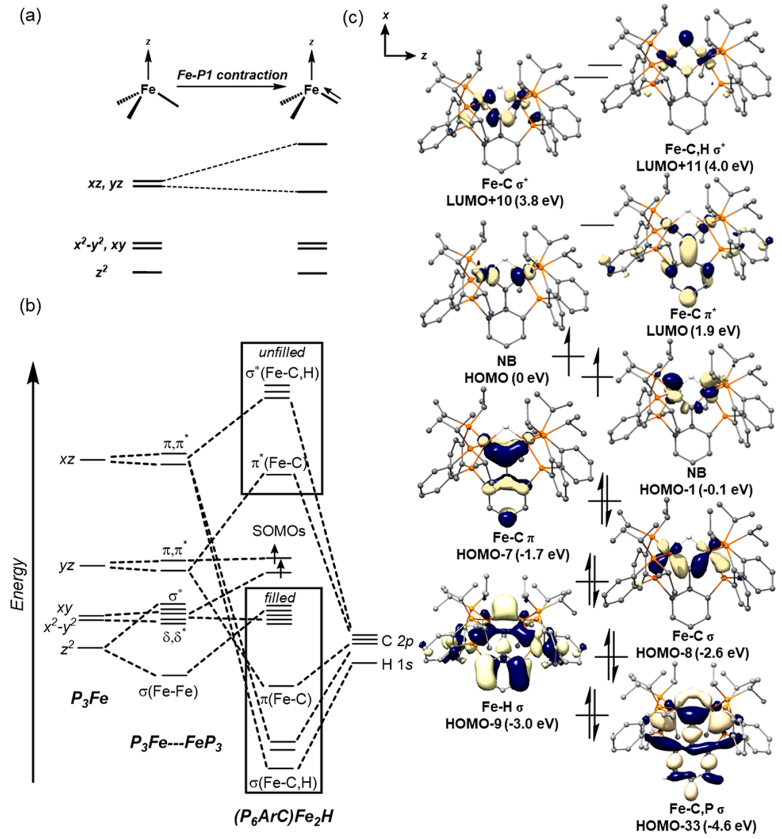

Figure 4. Electronic structure of $(P_6ArC)Fe_2(\mu\text{-H})$ (**5**). (a) Illustration of the effect of the contraction of the Fe1−P1 distance on the FMO's of the P_3Fe fragment. (b) Qualitative MO diagram for $(P_6ArC)Fe_2(\mu\text{-H})$ (**5**). (c) Calculated valence MOs $(P_6ArC)Fe_2(\mu\text{-H})$ (**5**) highlighting the SOMO's and key Fe−C interactions. Isosurfaces are shown at the 0.03 eÅ^3 level and orbital energies (relative to the HOMO) are provided.

Scheme 2. Mechanism for the Activation of 5 toward N_2 Binding

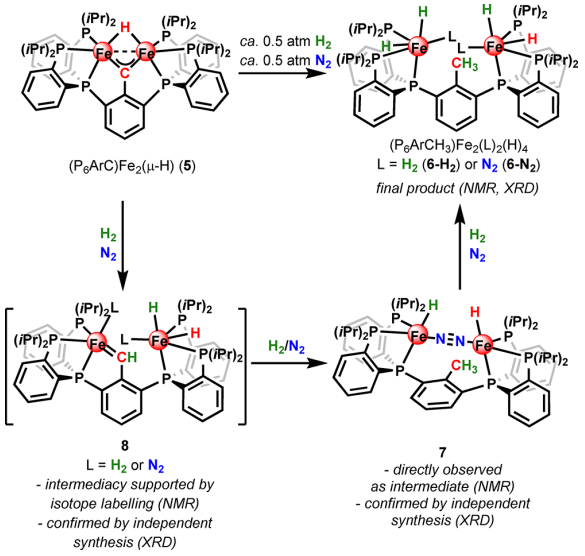

T_1 = 380 ms). The ATR-IR spectrum of **6-N_2** features diagnostic vibrational features at 2073 and 1790 cm^{-1} (Figure S35), corresponding to the N_2 and hydride ligands, respectively. Diffraction studies on **6-N_2** (Figure 5) confirm

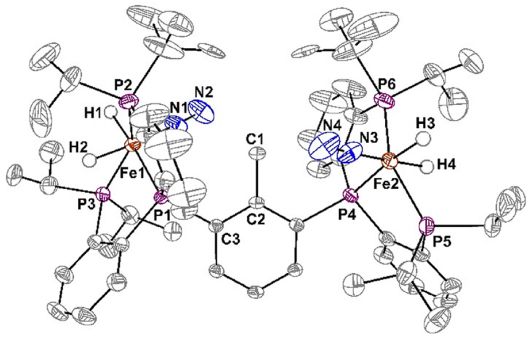

Figure 5. Crystal structure of $(P_6ArCH_3)Fe_2(N_2)_2(H)_4$(**6**). Hydrogen atoms on the ligand are omitted for clarity. Thermal ellipsoids shown at 50% probability.

that the central carbon has been fully hydrogenated (Fe1−C1:3.983(3) Å, Table S7). Each iron center in **6-N_2** is six-coordinate, with one hydride bisecting the equatorial phosphine donors (P2−F1−P3:146.72(5)°). The other hydride is trans to the unique phosphine ligand P1.

https://dx.doi.org/10.1021/jacs.0c01896
J. Am. Chem. Soc. 2020, 142, 10059−10068

Overall, the formation of **6** involves the addition of 3 equiv of H_2 to **5**. To better understand the activation process, we sought to identify relevant intermediates. In situ monitoring of the reaction via ^{31}P NMR spectroscopy facilitates detection of one diamagnetic intermediate (Figure S48). This species exhibits three distinct ^{31}P resonances (δ = 126.4 ppm, 2P; 121.3 ppm; 2P, 110.8 ppm, 2P), indicating a loss of front-back mirror symmetry with respect to **5**. Although this intermediate cannot be isolated directly from the reaction of **5** with H_2, a compound with identical ^{1}H and ^{31}P NMR features can be independently prepared (Scheme 3). This species is accessed

Scheme 3. Independent Synthesis of 7 and 8

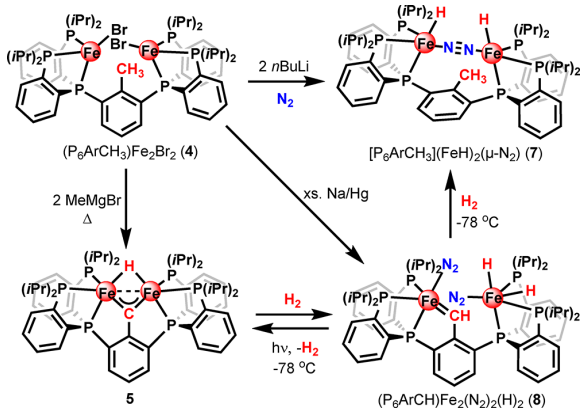

by reaction of **4** with 2 equiv of *n*BuLi, and was identified as the diiron(I) μ-κ^1:κ^1-N_2 dihydride complex $[P_6ArCH_3](FeH)_2(\mu\text{-}N_2)$ (**7**) by XRD analysis (Figure 6a). The most noteworthy feature of the solid state structure of **7** is the ligand distortion (C1−C2−C3−P1 torsion angle: 29.8(5)°, Table S7) necessary to accommodate the Fe−N_2−Fe linkage. Otherwise, it resembles a previously reported, untethered congener, which also reacts with H_2 to generate an $Fe(H)_2(N_2)$ complex following exposure to N_2.[64,65] The singlet ground state of **7** likely arises from antiferromagnetic coupling of two low spin Fe(I) centers through the linear N_2 bridge.[64] Generation of the intermediate **7** requires the addition of 2 equiv of H_2 to **5**, with the central carbyne ligand being fully protonated.

Efforts to directly observe the intermediate resulting from addition of only 1 equiv of H_2 to **5** during the course of the reaction were not fruitful. However, isotope labeling experiments provide insight into the mechanism of this transformation. When **5** is exposed to a mixture of D_2 and N_2, a feature at −12.9 ppm integrating to one proton is observed in the ^{1}H NMR spectrum of the product **6** (Figure S52). Moreover, no signal corresponding to a $-CHD_2$ group is observed, demonstrating that D_2 adds regioselectively across one Fe−C bond with the original hydride ligand of **5** remaining bound to Fe. At room temperature under ambient light, this reaction is not reversible and the original hydride ligand of **5** does not exchange with D_2 in the headspace.

The foregoing experiment indicates that the intermediate arising from addition of 1 equiv of H_2 to **5** has formed at least one C−H bond and has at least one iron-bound hydride. Such a species can be independently synthesized by reduction of the diiron(I) dibromide **4** with excess Na/Hg amalgam (Scheme 3), affording the diiron(II) carbene, dihydride complex $(P_6ArCH)Fe_2(N_2)_2(H)_2$ (**8**, Figure 6b). One iron site has trigonal bipyramidal symmetry, with an N_2 ligand located trans to P1. The central carbon is bound to this iron via a terminal Fe=C(*H*)Ar linkage, characterized by a short Fe1−C1 distance (1.911(4) Å, Table S7). A detailed investigation of the electronic structure of **8** is beyond the scope of the present study, but we note the relatively long iron-carbene bond length that may implicate an unusual electron configuration at Fe1.[66] The other iron center is six coordinate, with a *cis*-dihydride motif. One hydride ligand bisects the P5−Fe2−P6 angle (151.36(5)°) while the other is trans to P4.

The presence of a terminal Fe=C(*H*)Ar motif in **8** is indicated by a diagnostic resonance at δ = 11.0 ppm (s, 1H) in the ^{1}H NMR spectrum (Figure S40). The carbon atom of Fe=*C*(H)R linkage gives rise to a strongly upfield shifted resonance, which appears as a 1:2:2:2:1 quintet at δ = 224 ppm in the $^{13}C\{^{1}H\}$ NMR spectrum due to coupling to two inequivalent classes of phosphorus nuclei ($^{2}J_{C-P}$ = 40 Hz, 1P; $^{2}J_{C-P}$ = 20 Hz, 2P). This feature becomes a doublet of quintets in the gate-decoupled ^{13}C NMR spectrum (Figure S44) due to coupling to the Fe=C(*H*)R proton ($^{1}J_{C-H}$ = 134 Hz). Spectroscopic confirmation of the presence of two iron-bound hydride ligands is obtained from the ^{1}H NMR spectrum of **8**, which features characteristic resonances at δ = −9.7 ppm and −20.6 ppm each corresponding to one proton (Figures S40 and S41). The hydride ligands are also detectable by IR spectroscopy, giving rise to a broad ν_{Fe-H} feature at 1789 cm^{-1}. Additional resonances at 2006 and 2070 cm^{-1} arise from the two molecules of N_2 observed in the solid state structure of **8**,

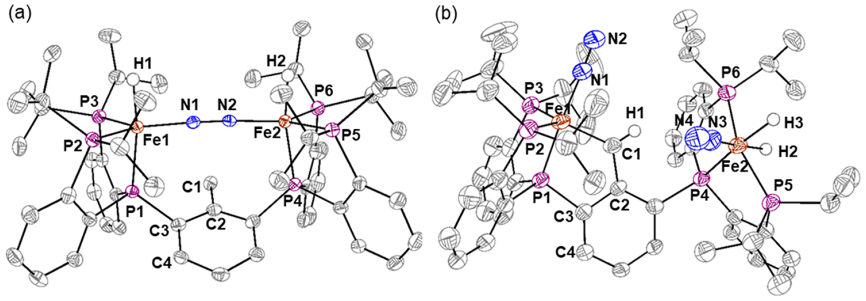

Figure 6. Independent synthesis of $[P_6ArCH_3](FeH)_2(\mu\text{-}N_2)$ (**7**) and $(P_6ArCH)Fe_2(N_2)_2(H)_2$ (**8**) from $(P_6ArCH_3)Fe_2Br_2$ (**4**). (a) Crystal structure of $[P_6ArCH_3](FeH)_2(\mu\text{-}N_2)$ (**7**). (b) Crystal structure of $(P_6ArCH)Fe_2(N_2)_2(H)_2$ (**8**). Hydrogen atoms on the ligand are omitted for clarity. Thermal ellipsoids shown at 50% probability.

https://dx.doi.org/10.1021/jacs.0c01896
J. Am. Chem. Soc. 2020, 142, 10059−10068

one at each iron (Figure S45). Beyond its relevance to the activation of **5** toward coordination of N_2, **8** is a rare example of an N_2-bound iron−carbene or−alkylidene complex, with only one series of compounds reported previously.[27]

The carbene complex **8** is a kinetically competent intermediate in the hydrogenation of **5**. Reaction of **8** with an equimolar mixture of H_2 and N_2 proceeds much more rapidly than the corresponding reaction of **5** (Figures S59 and S60). However, the initial product of this transformation is not **6-H$_2$**, but rather an equivalent species exhibiting mixed H_2/N_2 coordination (**6-H$_2$/N$_2$**). Evidently, N_2 does not readily exchange with H_2 under the experimental conditions. This notion is supported by the fact that **6-H$_2$/N$_2$** gradually converts to **6−N$_2$** upon exposure to an atmosphere of N_2 (Figures S61 and S62), similar to what is observed for **6-H$_2$**. Additional support for the intermediacy[67] of **8** in the hydrogenation of **5** was obtained by demonstrating that the reverse process−liberation of H_2 to generate **5**—is feasible under photolytic conditions (Scheme 3 and Figure S64). If the photolysis of **8** is conducted at −78 °C, then both **5** and **7** are produced simultaneously (Figures S65 and S66). The most probable origin of **7** in these experiments is from addition of H_2 (liberated during the photolysis) to residual **8**, rather than addition of 2 equiv of H_2 to **5** (Scheme 3). Indeed, independent studies show that **5** does not react with H_2/N_2 at low temperatures. Attempts to stoichiometrically add H_2 to **8** otherwise have consistently led to over-reaction to **6**. However, slow in situ generation of H_2 via photolysis was a convenient strategy to observe conversion of **8** to **7**, the next intermediate in sequence.

Consequences for H_2 and N_2 Activation. Paramagnetic complexes which bind[68−70] and cleave[63,71−73] H_2 remain rare. In a well-characterized example, Rh^{II} porphyrin complexes split H_2 via a linear, termolecular $[M\cdots H\cdots H\cdots M]^{‡}$ transition state.[74,75] This linear transition state facilitates homolytic cleavage by optimizing both M···H interactions in a manner similar to that implicated for other radical-type atom abstraction reactions.[75] In contrast, the spin-carrying orbitals of **5** are orthogonal (Figure 4), which precludes direct diradical activation of H_2 from **5**. Instead, H−H cleavage by **5** likely involves a transient σ-complex (Scheme 4). This intermediate

Scheme 4. Plausible Mechanisms for H_2 Activation by 5

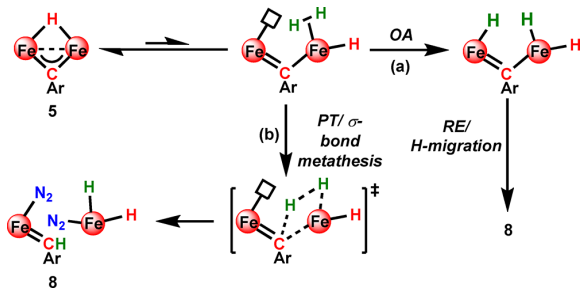

may undergo bimetallic oxidative addition[76] followed rapidly by C−H bond formation (reductive elimination/H-migration) to avoid the accumulation of a spectroscopically observable trihydride intermediate, affording **8** (pathway a in Scheme 4). Moreover, this OA/RE sequence has to be irreversible (i.e., RE must be fast relative to OA), otherwise the original μ-hydride ligand would scramble and be statistically incorporated into the incipient methyl group, which is not observed experimentally. This scenario would be in contrast with the rapid interconversion of hydride and H_2 ligands that occurs in **6-H2**.

An alternative mechanism for the formation of **8** involves concerted cleavage of H_2 and formation of the C−H bond (pathway b in Scheme 4). In this mechanism, displacement of the μ-hydride facilitates an intramolecular formal deprotonation of H_2 by the μ-carbyne ligand (or, as an alternative, a σ-bond metathesis, which would involve a similar transition state), converting **5** directly to the carbene-dihydride complex **8**. The lack of H/D scrambling into $-CH_3$ substituent implies that this deprotonation is irreversible, at least under thermal conditions, suggesting that the basicity of the μ-carbyne ligand may drive the reaction.

Although hydrogenation of **5** is thermodynamically favorable, it is a remarkably slow process, proceeding to completion only over the course of days. In contrast, cleavage of H_2 by the diamagnetic tetrairon μ_4-carbide cluster $[Fe_4C(CO)_{12}]^{2-}$ proceeds rapidly, even at lower temperatures.[77] Likwise, a diamagnetic diiron(II) μ-nitride complex $[([PhBP_3]Fe)_2(\mu\text{-}N)][Na(THF)_5]$, readily activates H_2, with full conversion to the μ-imide, μ-hydride species $[([PhBP_3]Fe)_2(\mu\text{-}NH)(\mu\text{-}H)][Na(THF)_5]$ within 30 min.[59] This latter species, although isoelectronic to **5**, appears to be inert to H_2, consistent with the suggestion that the enhanced basicity of the μ-carbyne is crucial for the observed reactivity.

The experimental data suggest that conversion of the open-shell diiron μ-carbyne complex **5** to the diamagnetic iron-carbene species **8** is the rate-limiting step in the overall transformation of **5** to **6**. As such, the slow overall reaction kinetics may result from the spin-forbidden character of this first H_2 activation step (see Figure S76 for a representation of the initial σ-interaction of the incoming H_2 ligand with the $3d_{x2-y2}$-derived orbital HOMO-1, a potential site of incoming ligand coordination). Along the reaction coordinate for ligand binding in **5**, the ground state may mix with a singlet excited state in which this orbital is unoccupied, thereby introducing a spin-induced kinetic barrier.[78,79] Such barriers are avoided in the interconversion of $2H^+/H_2$ by the hydrogenase enzymes due to the low-spin character of the active sites, which are stabilized by their CO and $^-$CN rich coordination environment.[80]

Delivery of reducing equivalents to paramagnetic active sites via discrete $1H^+/1e^-$ transfer events may be kinetically advantageous as it avoids additional barriers due to changes in overall spin state. Indeed, reductive activation of FeMoco involves discrete proton/electron transfer events,[1] although several reduced forms of the cofactor can also be reversibly interconverted via addition/loss of H_2.[81−85] Preliminary experiments demonstrate that addition of PCET reagents (e.g., TEMPO-H) or acids (e.g., HCl) to **5** also yields species which bind N_2 concomitant with Fe−C bond cleavage and C−H bond formation (Scheme 5). For example, treatment of **5** with TEMPO-H affords a mixture of species, only one of which exhibits well-defined ^{31}P NMR signals. The ^1H NMR of the reaction mixture reveals a diagnostic Fe=C(*H*)R resonance at 11.7 ppm for this diamagnetic species (Figure S69). Coordination of N_2 by this compound is suggested by the observation of a feature at 2076 cm^{-1} in the IR spectrum (Figure S71). Alternatively, protonation of **5** with HCl proceeds more cleanly, yielding a new paramagnetic species identified as the alkyliron(II)−N_2, iron(I)−chloride complex $(P_6ArCH_2)Fe(N_2)FeCl$ (**9**) by XRD analysis (Figure S71).

https://dx.doi.org/10.1021/jacs.0c01896
J. Am. Chem. Soc. 2020, 142, 10059−10068

Scheme 5. One or Two C−H Protonation Events, with Cleavage of one Fe−C Linkage, Promotes N_2 Binding

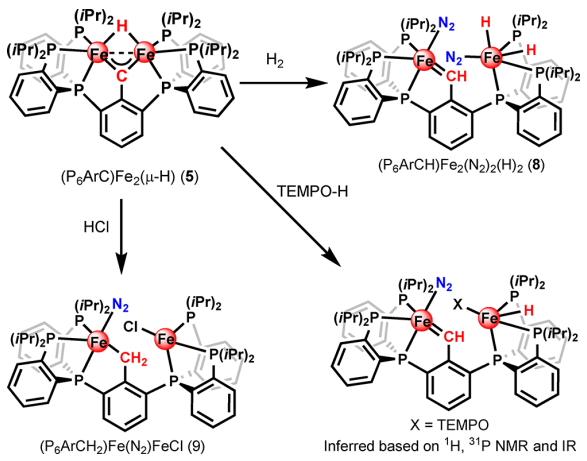

Although reaction of **5** with HCl proceeds rapidly, hydrogen atom abstraction from TEMPO-H is considerably slower. While the slower kinetics of this latter reaction may be partially attributed to a spin-induced kinetic barrier, the effects of sterics and polarity are difficult to assess. As a final comment, one has to note that the intriguing speculations above regarding the impact of spin state on the chemistry of **5** would require rigorous investigations to prove which are beyond the scope of this report.

The absence of direct N_2 coordination by **5** is also noteworthy. One can envision an isomer of **5** featuring a terminal hydride ligand that binds N_2 in an end-on fashion (analogous to the H_2 σ-complex illustrated in Scheme 4) or cooperatively between the two iron sites. This scenario seems all the more plausible given that a series of thiolate-bridged diiron complexes structurally related to **5** have been reported which readily bind N_2.[86] If such an isomer were the lowest in energy, then it seems likely that it would be accessible at the elevated reaction temperatures employed in the synthesis of **5**. Although spin-blocking might rationalize slow N_2 binding kinetics, there is evidently a thermodynamic perference for the μ-hydride ligand in **5**, in spite of the distortions it imposes on the ligand framework. Whether this thermodynamic bias against N_2 binding is predominantly electronic or steric in origin, our studies clearly demonstrate that displacement of the μ-hydride via C−H bond formation is a viable mechanism to promote an otherwise unfavorable N_2 coordination event.

CONCLUSIONS

Although it is difficult to harmonize the entirety of Siegbahn's mechanism[19] with the fact that the interstitial carbide is neither exchanged nor lost during turnover,[87] our studies demonstrate that Fe−C bond cleavage and C−H bond formation is a feasible mechanism for activation of a carbon-bridged diiron site toward binding N_2. The open shell diiron μ-carbyne complex **5** does not bind N_2 on its own, emphasizing the robustness of the Fe(μ-X)$_2$Fe (X = C, H, or S) diamond core motif. Coordination of N_2 at such a subsite evidently requires cleavage of at least one Fe−X bond, although the effect of the higher coordination number of **5** and its sterically congested environment on N_2 binding remain under investigation. While intermediates such as **7** featuring a fully protonated carbon bind N_2, a single C−H protonation event, with concomitant cleavage of one Fe−C bond, is sufficient to generate a site which coordinates N_2. Given that the μ_6-C^{4-} ligand of FeMoco is installed via C−H activation, monoprotonation of the carbide may be reversible and generate an intermediate sufficiently reactive that it has avoided direct spectroscopic detection to date.

ASSOCIATED CONTENT

Supporting Information

The Supporting Information is available free of charge at https://pubs.acs.org/doi/10.1021/jacs.0c01896.

Crystal data (CIF)

Synthetic procedures, characterization data, reactivity studies, and computational results (PDF)

AUTHOR INFORMATION

Corresponding Author

Theodor Agapie − *Division of Chemistry and Chemical Engineering, California Institute of Technology, Pasadena, California 91125, United States;* orcid.org/0000-0002-9692-7614; Email: agapie@caltech.edu

Author

Charles H. Arnett − *Division of Chemistry and Chemical Engineering, California Institute of Technology, Pasadena, California 91125, United States;* orcid.org/0000-0002-1272-3797

Complete contact information is available at: https://pubs.acs.org/10.1021/jacs.0c01896

Notes

The authors declare no competing financial interest.

ACKNOWLEDGMENTS

We are grateful to the NSF for funding (CHE-1905320 to T.A. and an NSF Graduate Research Fellowship to C.H.A.). We thank Prof. Jonas C. Peters for insightful discussions and for the use of his group's Mössbauer spectrometer. We thank Michael Takase and Lawrence Henling for assistance with X-ray crystallography and David VanderVelde for assistance with NMR spectroscopy. Magnetic data was acquired at the University of California, Los Angeles with assistance from Dr. Ignacio Martini on a Quantum Design MPMS3 SQUID Magnetometer supported by the NSF (MRI-1625776). The Dow Next Generation Educator Fund is acknowledged for X-ray diffraction and NMR instrumentation. The computations presented here were conducted on the Caltech High Performance Cluster partially supported by a grant from the Gordon and Betty Moore Foundation.

REFERENCES

(1) Hoffman, B. M.; Lukoyanov, D.; Yang, Z.-Y.; Dean, D. R.; Seefeldt, L. C. Mechanism of Nitrogen Fixation by Nitrogenase: The Next Stage. *Chem. Rev.* **2014**, *114* (8), 4041−4062.

(2) Spatzal, T.; Aksoyoglu, M.; Zhang, L.; Andrade, S. L. A.; Schleicher, E.; Weber, S.; Rees, D. C.; Einsle, O. Evidence for Interstitial Carbon in Nitrogenase FeMo Cofactor. *Science* **2011**, *334* (6058), 940−940.

(3) Einsle, O.; Tezcan, F. A.; Andrade, S. L. A.; Schmid, B.; Yoshida, M.; Howard, J. B.; Rees, D. C. Nitrogenase MoFe-Protein at 1.16 Å Resolution: A Central Ligand in the FeMo-Cofactor. *Science* **2002**, *297* (5587), 1696−1700.

(4) Kirn, J.; Rees, D. C. Crystallographic structure and functional implications of the nitrogenase molybdenum-iron protein from Azotobacter vinelandii. *Nature* **1992**, *360*, 553.
(5) Lancaster, K. M.; Roemelt, M.; Ettenhuber, P.; Hu, Y.; Ribbe, M. W.; Neese, F.; Bergmann, U.; DeBeer, S. X-ray Emission Spectroscopy Evidences a Central Carbon in the Nitrogenase Iron-Molybdenum Cofactor. *Science* **2011**, *334* (6058), 974−977.
(6) Igarashi, R. Y.; Laryukhin, M.; Dos Santos, P. C.; Lee, H.-I.; Dean, D. R.; Seefeldt, L. C.; Hoffman, B. M. Trapping H- Bound to the Nitrogenase FeMo-Cofactor Active Site during H_2 Evolution: Characterization by ENDOR Spectroscopy. *J. Am. Chem. Soc.* **2005**, *127* (17), 6231−6241.
(7) Lukoyanov, D.; Yang, Z.-Y.; Dean, D. R.; Seefeldt, L. C.; Hoffman, B. M. Is Mo Involved in Hydride Binding by the Four-Electron Reduced (E4) Intermediate of the Nitrogenase MoFe Protein? *J. Am. Chem. Soc.* **2010**, *132* (8), 2526−2527.
(8) Buscagan, T. M.; Rees, D. C. Rethinking the Nitrogenase Mechanism: Activating the Active Site. *Joule* **2019**, *3* (11), 2662−2678.
(9) Čorić, I.; Holland, P. L. Insight into the Iron-Molybdenum Cofactor of Nitrogenase from Synthetic Iron Complexes with Sulfur, Carbon, and Hydride Ligands. *J. Am. Chem. Soc.* **2016**, *138* (23), 7200−7211.
(10) Lee, S. C.; Lo, W.; Holm, R. H. Developments in the Biomimetic Chemistry of Cubane-Type and Higher Nuclearity Iron-Sulfur Clusters. *Chem. Rev.* **2014**, *114* (7), 3579−3600.
(11) Venkateswara Rao, P.; Holm, R. H. Synthetic Analogues of the Active Sites of Iron-Sulfur Proteins. *Chem. Rev.* **2004**, *104* (2), 527−560.
(12) Spatzal, T.; Perez, K. A.; Einsle, O.; Howard, J. B.; Rees, D. C. Ligand binding to the FeMo-cofactor: Structures of CO-bound and reactivated nitrogenase. *Science* **2014**, *345* (6204), 1620−1623.
(13) Spatzal, T.; Perez, K. A.; Howard, J. B.; Rees, D. C. Catalysis-dependent selenium incorporation and migration in the nitrogenase active site iron-molybdenum cofactor. *eLife* **2015**, *4*, No. e11620.
(14) Sippel, D.; Rohde, M.; Netzer, J.; Trncik, C.; Gies, J.; Grunau, K.; Djurdjevic, I.; Decamps, L.; Andrade, S. L. A.; Einsle, O. A bound reaction intermediate sheds light on the mechanism of nitrogenase. *Science* **2018**, *359* (6383), 1484−1489.
(15) Varley, J. B.; Wang, Y.; Chan, K.; Studt, F.; Nørskov, J. K. Mechanistic insights into nitrogen fixation by nitrogenase enzymes. *Phys. Chem. Chem. Phys.* **2015**, *17* (44), 29541−29547.
(16) Dance, I. How feasible is the reversible S-dissociation mechanism for the activation of FeMo-co, the catalytic site of nitrogenase? *Dalton Trans.* **2019**, *48* (4), 1251−1262.
(17) Čorić, I.; Mercado, B. Q.; Bill, E.; Vinyard, D. J.; Holland, P. L. Binding of dinitrogen to an iron-sulfur-carbon site. *Nature* **2015**, *526*, 96.
(18) Siegbahn, P. E. M. The mechanism for nitrogenase including all steps. *Phys. Chem. Chem. Phys.* **2019**, *21* (28), 15747−15759.
(19) Siegbahn, P. E. M. Model Calculations Suggest that the Central Carbon in the FeMo-Cofactor of Nitrogenase Becomes Protonated in the Process of Nitrogen Fixation. *J. Am. Chem. Soc.* **2016**, *138* (33), 10485−10495.
(20) McKee, M. L. A New Nitrogenase Mechanism Using a CFe_8S_9 Model: Does H_2 Elimination Activate the Complex to N_2 Addition to the Central Carbon Atom? *J. Phys. Chem. A* **2016**, *120* (5), 754−764.
(21) Speelman, A. L.; Čorić, I.; Van Stappen, C.; DeBeer, S.; Mercado, B. Q.; Holland, P. L. Nitrogenase-Relevant Reactivity of a Synthetic Iron-Sulfur-Carbon Site. *J. Am. Chem. Soc.* **2019**, *141* (33), 13148−13157.
(22) Hickey, A. K.; Muñoz, S. B.; Lutz, S. A.; Pink, M.; Chen, C.-H.; Smith, J. M. Arrested α-hydride migration activates a phosphido ligand for C-H insertion. *Chem. Commun.* **2017**, *53* (2), 412−415.
(23) Creutz, S. E.; Peters, J. C. Catalytic Reduction of N_2 to NH_3 by an Fe-N_2 Complex Featuring a C-Atom Anchor. *J. Am. Chem. Soc.* **2014**, *136* (3), 1105−1115.
(24) Rittle, J.; Peters, J. C. Fe-N_2/CO complexes that model a possible role for the interstitial C atom of FeMo-cofactor (FeMoco). *Proc. Natl. Acad. Sci. U. S. A.* **2013**, *110* (40), 15898−15903.
(25) Reiners, M.; Baabe, D.; Zaretzke, M.-K.; Freytag, M.; Walter, M. D. Reversible dinitrogen binding to [Cp′Fe(NHC)] associated with an N_2-induced spin state change. *Chem. Commun.* **2017**, *53* (53), 7274−7277.
(26) Ouyang, Z.; Cheng, J.; Li, L.; Bao, X.; Deng, L. High-Spin Iron(I) and Iron(0) Dinitrogen Complexes Supported by N-Heterocyclic Carbene Ligands. *Chem. - Eur. J.* **2016**, *22* (40), 14162−14165.
(27) Lindley, B. M.; Jacobs, B. P.; MacMillan, S. N.; Wolczanski, P. T. Neutral Fe(iv) alkylidenes, including some that bind dinitrogen. *Chem. Commun.* **2016**, *52* (20), 3891−3894.
(28) Ung, G.; Peters, J. C. Low-Temperature N_2 Binding to Two-Coordinate L_2Fe^0 Enables Reductive Trapping of $L_2FeN_2^-$ and NH_3 Generation. *Angew. Chem., Int. Ed.* **2015**, *54* (2), 532−535.
(29) Marchetti, F. Constructing Organometallic Architectures from Aminoalkylidyne Diiron Complexes. *Eur. J. Inorg. Chem.* **2018**, *2018* (36), 3987−4003.
(30) Vollmer, G. Y.; Wallasch, M. W.; Saurenz, D.; Eger, T. R.; Bauer, H.; Wolmershäuser, G.; Prosenc, M. H.; Sitzmann, H. Benzylidyne Bridges from Diphenylacetylene and a Methylidyne Bridge from Methylmagnesium Chloride. *Organometallics* **2015**, *34* (3), 644−652.
(31) Xiao, N.; Xu, Q.; Sun, J.; Chen, J. Synthesis, structure and reactivity of novel pyridazine-coordinated diiron bridging carbene complexes. *Dalton Trans.* **2005**, No. 19, 3250−3258.
(32) Chen, J.; Wang, R. Remarkable reactions of cationic carbyne complexes of manganese, rhenium, and diiron with carbonylmetal anions. *Coord. Chem. Rev.* **2002**, *231* (1), 109−149.
(33) Albano, V. G.; Busetto, L.; Monari, M.; Zanotti, V. Reactions of acetonitrile di-iron μ-aminocarbyne complexes; synthesis and structure of $[Fe_2(\mu\text{-}CNMe_2)(\mu\text{-}H)(CO)_2(Cp)_2]$. *J. Organomet. Chem.* **2000**, *606* (2), 163−168.
(34) Holton, J.; Lappert, M. F.; Pearce, R.; Yarrow, P. I. W. Bridged hydrocarbyl or hydrocarbon binuclear transition metal complexes: classification, structures, and chemistry. *Chem. Rev.* **1983**, *83* (2), 135−201.
(35) Casey, C. P.; Fagan, P. J.; Miles, W. H. Synthesis and interconversions of dinuclear iron complexes with μ-methyl, μ-methylene, and μ-methylidyne ligands. *J. Am. Chem. Soc.* **1982**, *104* (4), 1134−1136.
(36) Nitay, M.; Priester, W.; Rosenblum, M. Lithium ion promotion in the synthesis of novel dinuclear iron-carbyne complexes. *J. Am. Chem. Soc.* **1978**, *100* (11), 3620−3622.
(37) Casey, C. P.; Roddick, D. M. Formation of a bridging methylidyne complex and of a bridging vinyl complex from the reaction of $[(C_5H_5)Fe(NO)]_2(\mu\text{-}CH_2)$ with trityl cation. *Organometallics* **1986**, *5* (3), 436−438.
(38) Busetto, L.; Zanotti, V. Carbene ligands in diiron complexes. *J. Organomet. Chem.* **2005**, *690* (24), 5430−5440.
(39) Casey, C. P.; Vosejpka, P. C.; Crocker, M. Reactions of nucleophiles with cationic bridging alkylidyne complexes. *J. Organomet. Chem.* **1990**, *394* (1), 339−347.
(40) Casey, C. P.; Meszaros, M. W.; Fagan, P. J.; Bly, R. K.; Marder, S. R.; Austin, E. A. Hydrocarbation-formation of diiron μ-alkylidyne complexes from the addition of the carbon-hydrogen bond of a μ-methylidyne complex across alkenes. *J. Am. Chem. Soc.* **1986**, *108* (14), 4043−4053.
(41) Bursten, B. E.; Cayton, R. H. Electronic structure of piano-stool dimers. 3. Relationships between the bonding and reactivity of the organically bridged iron dimers $[CpFe(CO)]_2(\mu\text{-}CO)(\mu\text{-}L)$ (L = CO, CH2, C = CH_2, CH^+). *J. Am. Chem. Soc.* **1986**, *108* (26), 8241−8249.
(42) Casey, C. P.; Fagan, P. J.; Miles, W. H.; Marder, S. R. Reactions of a cationic bridging methylidyne-iron complex with carbon monoxide and with alkenes. *J. Mol. Catal.* **1983**, *21* (1), 173−188.
(43) Casey, C. P.; Fagan, P. J.; Day, V. W. Formation of the bridging acylium complex $(C_5H_5)_2Fe_2(CO)_2(\mu\text{-}CO)(\mu\text{-}CHCO)^+$ PF_6^- by

https://dx.doi.org/10.1021/jacs.0c01896
J. Am. Chem. Soc. 2020, 142, 10059−10068

addition of carbon monoxide to a bridging methylidyne-iron complex. *J. Am. Chem. Soc.* **1982**, *104* (25), 7360−7361.
(44) Casey, C. P.; Fagan, P. J. Hydrocarbation: addition of the carbon-hydrogen bond of a cationic bridging iron-methylidyne complex to alkenes. *J. Am. Chem. Soc.* **1982**, *104* (18), 4950−4951.
(45) Reesbeck, M. E.; Grubel, K.; Kim, D.; Brennessel, W. W.; Mercado, B. Q.; Holland, P. L. Diazoalkanes in Low-Coordinate Iron Chemistry: Bimetallic Diazoalkyl and Alkylidene Complexes of Iron(II). *Inorg. Chem.* **2017**, *56* (3), 1019−1022.
(46) Yogendra, S.; Weyhermüller, T.; Hahn, A. W.; DeBeer, S. From Ylides to Doubly Yldiide-Bridged Iron(II) High Spin Dimers via Self-Protolysis. *Inorg. Chem.* **2019**, *58* (14), 9358−9367.
(47) Sun, C.-L.; Krause, H.; Fürstner, A. A Practical Procedure for Iron-Catalyzed Cross-Coupling Reactions of Sterically Hindered Aryl-Grignard Reagents with Primary Alkyl Halides. *Adv. Synth. Catal.* **2014**, *356* (6), 1281−1291.
(48) Ni, C.; Power, P. P. Methyl-Bridged Transition Metal Complexes (M = Cr-Fe) Supported by Bulky Terphenyl Ligands. *Organometallics* **2009**, *28* (22), 6541−6545.
(49) Klose, A.; Solari, E.; Floriani, C.; Chiesi-Villa, A.; Rizzoli, C.; Re, N. Magnetic Properties Diagnostic for the Existence of Iron(II)-Iron(II) Bonds in Dinuclear Complexes Which Derive from Stepwise Insertion Reactions on Unsupported Iron-Aryl Bonds. *J. Am. Chem. Soc.* **1994**, *116* (20), 9123−9135.
(50) Rettberg, L. A.; Wilcoxen, J.; Lee, C. C.; Stiebritz, M. T.; Tanifuji, K.; Britt, R. D.; Hu, Y. Probing the coordination and function of Fe_4S_4 modules in nitrogenase assembly protein NifB. *Nat. Commun.* **2018**, *9* (1), 2824.
(51) Wiig, J. A.; Hu, Y.; Ribbe, M. W. Refining the pathway of carbide insertion into the nitrogenase M-cluster. *Nat. Commun.* **2015**, *6* (1), 8034.
(52) Wiig, J. A.; Hu, Y.; Lee, C. C.; Ribbe, M. W. Radical SAM-Dependent Carbon Insertion into the Nitrogenase M-Cluster. *Science* **2012**, *337* (6102), 1672−1675.
(53) Hickey, A. K.; Greer, S. M.; Valdez-Moreira, J. A.; Lutz, S. A.; Pink, M.; DeGayner, J. A.; Harris, T. D.; Hill, S.; Telser, J.; Smith, J. M. A Dimeric Hydride-Bridged Complex with Geometrically Distinct Iron Centers Giving Rise to an $S = 3$ Ground State. *J. Am. Chem. Soc.* **2019**, *141* (30), 11970−11975.
(54) Yang, D.; Li, Y.; Wang, B.; Zhao, X.; Su, L.; Chen, S.; Tong, P.; Luo, Y.; Qu, J. Synthesis and Electrocatalytic Property of Diiron Hydride Complexes Derived from a Thiolate-Bridged Diiron Complex. *Inorg. Chem.* **2015**, *54* (21), 10243−10249.
(55) Lee, Y.; Anderton, K. J.; Sloane, F. T.; Ermert, D. M.; Abboud, K. A.; García-Serres, R.; Murray, L. J. Reactivity of Hydride Bridges in High-Spin [3M-3(μ-H)] Clusters (M = Fe^{II}, Co^{II}). *J. Am. Chem. Soc.* **2015**, *137* (33), 10610−10617.
(56) Arnet, N. A.; Dugan, T. R.; Menges, F. S.; Mercado, B. Q.; Brennessel, W. W.; Bill, E.; Johnson, M. A.; Holland, P. L. Synthesis, Characterization, and Nitrogenase-Relevant Reactions of an Iron Sulfide Complex with a Bridging Hydride. *J. Am. Chem. Soc.* **2015**, *137* (41), 13220−13223.
(57) Rittle, J.; McCrory, C. C. L.; Peters, J. C. A 10^6-Fold Enhancement in N_2-Binding Affinity of an $Fe_2(\mu\text{-H})_2$ Core upon Reduction to a Mixed-Valence $Fe^{II}Fe^{I}$ State. *J. Am. Chem. Soc.* **2014**, *136* (39), 13853−13862.
(58) Wang, W.; Nilges, M. J.; Rauchfuss, T. B.; Stein, M. Isolation of a Mixed Valence Diiron Hydride: Evidence for a Spectator Hydride in Hydrogen Evolution Catalysis. *J. Am. Chem. Soc.* **2013**, *135* (9), 3633−3639.
(59) Brown, S. D.; Mehn, M. P.; Peters, J. C. Heterolytic H_2 Activation Mediated by Low-Coordinate $L_3Fe\text{-}(\mu\text{-N})\text{-}FeL_3$ Complexes to Generate $Fe(\mu\text{-NH})(\mu\text{-H})Fe$ Species. *J. Am. Chem. Soc.* **2005**, *127* (38), 13146−13147.
(60) Neese, F. Prediction and interpretation of the ^{57}Fe isomer shift in Mössbauer spectra by density functional theory. *Inorg. Chim. Acta* **2002**, *337*, 181−192.
(61) Yao, S. A.; Corcos, A. R.; Infante, I.; Hillard, E. A.; Clérac, R.; Berry, J. F. An "Intermediate Spin" Nickel Hydride Complex Stemming from Delocalized $Ni_2(\mu\text{-H})_2$ Bonding. *J. Am. Chem. Soc.* **2014**, *136* (39), 13538−13541.
(62) Lee, Y.; Peters, J. C. Silylation of Iron-Bound Carbon Monoxide Affords a Terminal Fe Carbyne. *J. Am. Chem. Soc.* **2011**, *133* (12), 4438−4446.
(63) Prokopchuk, D. E.; Chambers, G. M.; Walter, E. D.; Mock, M. T.; Bullock, R. M. H_2 Binding, Splitting, and Net Hydrogen Atom Transfer at a Paramagnetic Iron Complex. *J. Am. Chem. Soc.* **2019**, *141* (5), 1871−1876.
(64) Buscagan, T. M.; Oyala, P. H.; Peters, J. C. N_2-to-NH_3 Conversion by a triphos-Iron Catalyst and Enhanced Turnover under Photolysis. *Angew. Chem., Int. Ed.* **2017**, *56* (24), 6921−6926.
(65) Schild, D. J.; Peters, J. C. Light Enhanced Fe-Mediated Nitrogen Fixation: Mechanistic Insights Regarding H_2 Elimination, HER, and NH_3 Generation. *ACS Catal.* **2019**, *9* (5), 4286−4295.
(66) Russell, S. K.; Hoyt, J. M.; Bart, S. C.; Milsmann, C.; Stieber, S. C. E.; Semproni, S. P.; DeBeer, S.; Chirik, P. J. Synthesis, electronic structure and reactivity of bis(imino)pyridine iron carbene complexes: evidence for a carbene radical. *Chem. Sci.* **2014**, *5* (3), 1168−1174.
(67) It is most likely that under the experimental conditions (equimolar H_2/N_2) for hydrogenation of **5** that intermediate **8** binds H_2 rather than N_2. If N_2 were to be bound, then **6-H_2/N_2** or **6-N_2** rather than **6-H_2** would be the expected product.
(68) Lee, Y.; Kinney, R. A.; Hoffman, B. M.; Peters, J. C. A Nonclassical Dihydrogen Adduct of $S = 1/2$ Fe(I). *J. Am. Chem. Soc.* **2011**, *133* (41), 16366−16369.
(69) Suess, D. L. M.; Tsay, C.; Peters, J. C. Dihydrogen Binding to Isostructural $S = 1/2$ and $S = 0$ Cobalt Complexes. *J. Am. Chem. Soc.* **2012**, *134* (34), 14158−14164.
(70) Doyle, L. R.; Scott, D. J.; Hill, P. J.; Fraser, D. A. X.; Myers, W. K.; White, A. J. P.; Green, J. C.; Ashley, A. E. Reversible coordination of N_2 and H_2 to a homoleptic $S = 1/2$ Fe(i) diphosphine complex in solution and the solid state. *Chem. Sci.* **2018**, *9* (37), 7362−7369.
(71) Dugan, T. R.; Holland, P. L. New routes to low-coordinate iron hydride complexes: The binuclear oxidative addition of H_2. *J. Organomet. Chem.* **2009**, *694* (17), 2825−2830.
(72) Halpern, J.; Pribanic, M. Hydrogenation of pentacyanocobaltate(II) at high pressures. *Inorg. Chem.* **1970**, *9* (11), 2616−2618.
(73) Tannenbaum, R.; Dietler, U. K.; Bor, G.; Ungváry, F. Fundamental metal carbonyl equilibria, V1 Reinvestigation of the equilibrium between dicobalt octacarbonyl and cobalt tetracarbonyl hydride under hydrogen pressure. *J. Organomet. Chem.* **1998**, *570* (1), 39−47.
(74) Cui, W.; Wayland, B. B. Activation of C-H/H-H Bonds by Rhodium(II) Porphyrin Bimetalloradicals. *J. Am. Chem. Soc.* **2004**, *126* (26), 8266−8274.
(75) Wayland, B. B.; Ba, S.; Sherry, A. E. Reactions of hydrogen or deuterium molecule with a rhodium(II) metalloradical: kinetic evidence for a four-centered transition state. *Inorg. Chem.* **1992**, *31* (1), 148−150.
(76) Manz, D.-H.; Duan, P.-C.; Dechert, S.; Demeshko, S.; Oswald, R.; John, M.; Mata, R. A.; Meyer, F. Pairwise H_2/D_2 Exchange and H_2 Substitution at a Bimetallic Dinickel(II) Complex Featuring Two Terminal Hydrides. *J. Am. Chem. Soc.* **2017**, *139* (46), 16720−16731.
(77) Davis, J. H.; Beno, M. A.; Williams, J. M.; Zimmie, J.; Tachikawa, M.; Muetterties, E. L. Structure and chemistry of a metal cluster with a four-coordinate carbide carbon atom. *Proc. Natl. Acad. Sci. U. S. A.* **1981**, *78* (2), 668−671.
(78) Carreón-Macedo, J.-L.; Harvey, J. N. Do Spin State Changes Matter in Organometallic Chemistry? A Computational Study. *J. Am. Chem. Soc.* **2004**, *126* (18), 5789−5797.
(79) Poli, R.; Harvey, J. N. Spin forbidden chemical reactions of transition metal compounds. New ideas and new computational challenges. *Chem. Soc. Rev.* **2003**, *32* (1), 1−8.
(80) Gordon, J. C.; Kubas, G. J. Perspectives on How Nature Employs the Principles of Organometallic Chemistry in Dihydrogen Activation in Hydrogenases. *Organometallics* **2010**, *29* (21), 4682−4701.

https://dx.doi.org/10.1021/jacs.0c01896
J. Am. Chem. Soc. 2020, 142, 10059−10068

(81) Lukoyanov, D. A.; Krzyaniak, M. D.; Dean, D. R.; Wasielewski, M. R.; Seefeldt, L. C.; Hoffman, B. M. Time-Resolved EPR Study of H_2 Reductive Elimination from the Photoexcited Nitrogenase Janus E_4(4H) Intermediate. *J. Phys. Chem. B* **2019**, *123* (41), 8823−8828.
(82) Lukoyanov, D.; Khadka, N.; Dean, D. R.; Raugei, S.; Seefeldt, L. C.; Hoffman, B. M. Photoinduced Reductive Elimination of H_2 from the Nitrogenase Dihydride (Janus) State Involves a FeMo-cofactor-H_2 Intermediate. *Inorg. Chem.* **2017**, *56* (4), 2233−2240.
(83) Lukoyanov, D.; Khadka, N.; Yang, Z.-Y.; Dean, D. R.; Seefeldt, L. C.; Hoffman, B. M. Reductive Elimination of H_2 Activates Nitrogenase to Reduce the N≡N Triple Bond: Characterization of the E_4(4H) Janus Intermediate in Wild-Type Enzyme. *J. Am. Chem. Soc.* **2016**, *138* (33), 10674−10683.
(84) Lukoyanov, D.; Khadka, N.; Yang, Z.-Y.; Dean, D. R.; Seefeldt, L. C.; Hoffman, B. M. Reversible Photoinduced Reductive Elimination of H_2 from the Nitrogenase Dihydride State, the E_4(4H) Janus Intermediate. *J. Am. Chem. Soc.* **2016**, *138* (4), 1320−1327.
(85) Lukoyanov, D.; Barney, B. M.; Dean, D. R.; Seefeldt, L. C.; Hoffman, B. M. Connecting nitrogenase intermediates with the kinetic scheme for N_2 reduction by a relaxation protocol and identification of the N_2 binding state. *Proc. Natl. Acad. Sci. U. S. A.* **2007**, *104* (5), 1451−1455.
(86) Creutz, S. E.; Peters, J. C. Diiron Bridged-Thiolate Complexes That Bind N_2 at the $Fe^{II}Fe^{II}$, $Fe^{II}Fe^{I}$, and $Fe^{I}Fe^{I}$ Redox States. *J. Am. Chem. Soc.* **2015**, *137* (23), 7310−7313.
(87) Wiig, J. A.; Lee, C. C.; Hu, Y.; Ribbe, M. W. Tracing the Interstitial Carbide of the Nitrogenase Cofactor during Substrate Turnover. *J. Am. Chem. Soc.* **2013**, *135* (13), 4982−4983.

https://dx.doi.org/10.1021/jacs.0c01896
J. Am. Chem. Soc. 2020, 142, 10059−10068